Optical monitoring of glutamate release at multiple synapses in situ detects changes following LTP induction

Olga Kopach
Queen Square Institute of Neurology, University College London
Kaiyu Zheng
Queen Square Institute of Neurology, University College London
Dmitri Rusakov (d.rusakov@ucl.ac.uk)
University College London https://orcid.org/0000-0001-9539-9947

Research

Keywords: Glutamate release, optical glutamate sensor, LTP, two-photon excitation imaging, acute hippocampal slices

Posted Date: December 23rd, 2019

DOI: https://doi.org/10.21203/rs.2.19455/v1

Version of Record: A version of this preprint was published at Molecular Brain on March 13th, 2020. See the published version at https://doi.org/10.1186/s13041-020-00572-x.

Abstract

Information processing and memory formation in the brain relies on release of the main excitatory neurotransmitter glutamate from presynaptic axonal specialisations. The classical Hebbian paradigm of synaptic memory, long-term potentiation (LTP) of transmission, has been widely associated with an increase in the postsynaptic receptor current. Whether and to what degree LTP induction also enhances presynaptic glutamate release has been the subject of debate. Here, we took advantage of the recently developed genetically encoded optical sensors of glutamate (iGluSnFr) to monitor its release at CA3-CA1 synapses in acute hippocampal slices, before and after the induction of LTP. We attempted to trace release events at multiple synapses simultaneously, by using two-photon excitation imaging in fast frame-scanning mode. We thus detected a significant increase in the average glutamate signal during potentiation, which lasted for up to 90 min.

Introduction

Hebbian postulates, which rationalise the principles of memory formation in the brain [1], have found their first experimental verification in the long-term potentiation (LTP) of excitatory transmission [2, 3]. The majority of excitatory synapses in the cortex operate by releasing glutamate from presynaptic axons, the process that underpins rapid information processing and storage by neural circuits. Following decades of debate, it has been argued that the prevailing cellular mechanism underlying LTP rests with an increased current through postsynaptic receptors [4]. Experimental evidence for the alternative hypothesis, such as an increase in glutamate release probability [5–7], has been countered by an elegant hypothesis of silent synapses [8, 9] and by documenting no increases in astroglial glutamate uptake post-induction [10, 11]. However, the LTP-associated boost of release probability at non-silent synapses has subsequently been reported [12, 13] whereas no change in overall glutamate release can reflect hetero-synaptic depression at non-active connections [14] or, more generally, rapid (pre)synaptic scaling [15, 16]. The uncertainty has remained, largely because documenting glutamate release at individual synapses has had to rely on its physiological consequences rather than on release readout per se.

The advent of FM dyes decades ago was an important step in providing optical tools to detect exocytosis of synaptic vesicles [17, 18]. More recently, the emergence of genetically encoded optical sensors for glutamate [19] has finally enabled direct monitoring of its release at individual synaptic connections. We showed earlier that, in certain imaging conditions, fluorescent glutamate 'sniffers' of the iGluSnFr family provide robust readout of glutamate release at identified synapses in organised brain tissue [20, 21], including in vivo [22]. In the present study, we take advantage of this approach in an attempt to understand changes in glutamate release properties at hippocampal Schaffer collateral axons, under the classical protocol of LTP induced by high-frequency afferent stimulation. We monitor LTP induction in the bulk of tissue, and analyse optical glutamate signals in arbitrary samples of presynaptic axonal boutons, which may correspond to both potentiated and non-potentiated synapses. In these settings, we aim to assess changes in glutamate release at individual synapses, and in the bulk of synaptic population.

Results

Viral delivery of iGluSnFr in neonates for multi-synapse glutamate imaging in situ

In our previous studies, we introduced optical glutamate sensors in the hippocampal neuropil via stereotaxic viral delivery in young animals [20] or via biolistic transfection in organotypic brain slices [21, 23]. However, brain injections in adults face challenges, such as potential interference with the tissue designated for acute slices, whereas the functional anatomy of organotypic slices might not fully represent that of intact tissue. We, therefore, sought to explore viral transduction in vivo via neonatal intracerebroventricular (ICV) injections (Fig. 1A), aiming at efficient transgene expression in neurons, for up to six weeks post-infection for subsequent ex vivo imaging.

We employed the new generation of AAV-based sensor variant with a relatively high off-rate, AAV9.hSynap.iGluSnFr.WPRE.SV40, but also used the recently described low off-rate sensor variant, SF-iGluSnFr.A184S [24] for comparison. Although AAV9 appeared to penetrate more readily after ICV administration [25] than did AAV2/1, at three to four weeks post-injection both methods provided efficient labelling of Schaffer collateral fragments in s. radiatum (Fig. 1B and 1C). The robust level of expression was maintained for at least six weeks post-infection, which made it suitable for ex vivo slice experiments in young adult animals.

To validate the method, we set out to monitor iGluSnFr fluorescence intensity integrated across the region of interest (incorporating several axonal boutons) during electric stimulation of Schaffer collaterals (five stimuli 50 ms apart; imaging settings as described earlier [20]). For time-lapse imaging, we employed frame-scanning mode providing rapid sampling rate (pixel dwell time 0.5 µs, frame time ~ 25 ms) across the area of interest (256 × 96 pixels, Fig. 1B). The recorded data sets were arranged as T-stacks, consisting of multiple frame scans (typically 35 to 50, depending on the duration of recording). We thus achieved reliable imaging of the dynamics of glutamate release across the sampled tissue fragment (Fig. 1C traces), with clear separation of five responses to individual electric stimuli (Fig. 1C; fEPSP and $\Delta F/F_0$ signal traces; one-trial example).

A similar experiment using the slow-unbinding A184S sensor variant (Fig. 1D) revealed robust reporting of stimulus-evoked rises in the iGluSnFr intensity (Fig. 1E). However, this approach did not seem to provide reliable separation between five responses to five individual stimuli at 20 Hz (Fig. 1E; $\Delta F/F_0$ trace, one-trial example), thus pointing to the corresponding limitations in temporal resolution.

Multi-synapse imaging of glutamate release at individual axonal boutons

We next asked if the chosen frame-scanning method is sufficiently sensitive to document glutamate release at in individual axonal boutons. We therefore used the recorded image-frame stacks to analyse fluorescence dynamics at small ROIs associated with individual axonal boutons (Fig. 2A). The fluorescence dynamics at individual selected boutons showed that recording sensitivity and signal-noise ratios were sufficient, in principle, to document individual glutamate releases (Fig. 2B; $\Delta F/F_0$ traces, four-

trial average). For comparison purposes, we recorded a fragment of the same axon (as Fig. 2A) in linescan mode, which provides high temporal resolution (~ 1.45 ms). The fluorescence dynamics thus recorded from three boutons of interest (Fig. 3A, bouton numbers as in Fig. 2A; one-trial example) was qualitatively similar to that obtained in the frame-scanning mode (compare boutons 5–7 in Fig. 2B and Fig. 3B).

Imaging of glutamate release during LTP induction

One of the main advantages of the frame-scan mode, as opposed to various linescan options, is relatively low laser exposure per pixel. Firstly, this lowers the propensity for irreversible photo-damage that may occur in cellular structures under intense laser light. Secondly, it reduces photobleaching of the fluorescent indicator, which has been a key prerequisite for stable longer-term imaging.

We therefore set out to explore this imaging method in an attempt to document changes, if any, of glutamate release during the high-frequency stimulation (HFS)-induced LTP. The classical LTP induction protocol in iGluSnFr-expressing acute slices produced a reliable increase in the fEPSP slope, lasting for over 80 min post-induction (example in Fig. 4A). In the selected areas of s. radiatum, we thus identified groups of candidate axonal boutons that remained firmly in focus during the experiment, to reduce any bias associated with focal drift (Fig. 4B). Unfortunately, the boutons selected based on this mandatory criterion, were not necessarily the boutons showing the best signal-to-noise ratios of their $\Delta F/F_0$ responses (as in Fig. 2). Whilst individual boutons displayed, if anything, varied effects of LTP induction on the fluorescence dynamics of iGluSnFR, they appeared to indicate a trend towards the increase in the $\Delta F/F_0$ signal amplitude (example in Fig. 4C).

This trend was more prominent when the area-integrated $\Delta F/F_0$ signals (as in Fig. 1C, E) were compared (Fig. 4D). To evaluate this effect quantitatively, we carried out paired comparisons, in which the difference was calculated between the average iGluSnFR $\Delta F/F_0$ traces recorded at 30 or 90 min post-induction, and those during baseline conditions prior to LTP induction. This analysis indicated a statistically significant increase in the optical glutamate signal amplitude following the induction of LTP (Fig. 4E). Whether this change necessarily indicates a greater amount of evoked glutamate release is discussed below.

Discussion

In this study, we took advantage of the recently developed, genetically encoded optical iGluSnFR sensors for glutamate [19, 24], in an attempt to detect changes in glutamate release following the induction of LTP. We have successfully transduced the sensors in hippocampal Schaffer collateral fibres using neonatal viral infection. We explored the suitability of the fast frame-scanning (two-photon excitation) imaging mode for monitoring optical glutamate signals from multiple axonal boutons, this identifying some advantages and limitations, in the context. The key advantage rests with the reduced exposure to laser light and the ability to record from multiple synaptic connections, in some cases with satisfactory sensitivity and temporal resolution. This is however somewhat offset by the fact that during longer- term

recordings and / or intense electric stimulation the tissue is likely to drift while also altering its morphological features, albeit on a microscopic scale. Because such movements could alter geometry and position of the fluorescence source(s), this could potentially bias the readout of dynamic optical recordings. Selecting the objects of interest, such as axonal boutons, based on their morphological stability potentially leads to suboptimal sampling in terms of the signal-to-noise ratio. The future improvements of the technique could combine more controlled, sparse labelling of axons with the vertically extended point-spread function (sometimes termed 'Bessel beam') of the two-photon excitation system. The latter should help overcome the effects of 3D drift, and therefore improve the sampling procedure.

Notwithstanding its potential limitations, the present approach has identified a significant increase in the average optical glutamate signal generated by Schaffer collateral axons after LTP induction. At first glance, this indicates an increased amount of released glutamate in response to afferent stimulation. However, the fluorescent signal of iGluSnFR reports glutamate molecules bound to the indicator. Any endogenous high-affinity glutamate buffer that competes with this binding process can potentially affects optical readout. Intriguingly, hippocampal neuropil is equipped with such a buffer, in the shape of high-affinity glutamate transporters that are expressed, at high density, on the surface of astroglia [26–28]. Thus, a significant decrease in the numbers of locally available glutamate transporters could boost the amount of glutamate binding to its optical sensor upon evoked release. Whether this is indeed the case is an intriguing and important question yet to be addressed. More generally, the remaining uncertainty regarding release probability changes during LTP is unlikely to be resolved unambiguously without considering the effects of LTP induction on both potentiated and (neighbouring) non-potentiated synapses, and possibly on the local astroglial microenvironment.

Methods

Viral transduction for labelling axonal boutons within CA3-CA1 region

All animal procedures were conducted in accordance with the European Commission Directive (86/609/EEC), the United Kingdom Home Office (Scientific Procedures) Act (1986). For the experiments, both male and female C57BL/6J mice (Charles River Laboratories) were used. For *ex vivo* imaging of individual boutons, an AAV virus expressing the neuronal optical glutamate sensor, AAV9.hSynap.iGluSnFr.WPRE.SV40, supplied by Penn Vector Core (PA, USA) was injected into the cerebral ventricles of neonates. For viral gene delivery, pups, male and female (P0-P1), were prepared for aseptic surgery. To ensure proper delivery, intracerebroventricular (ICV) injections were carried out after a sufficient visualization of the targeted area [29]. Viral particles were injected in a volume 2 ml/hemisphere (totalling 5 x 10^9 genomic copies), using a glass Hamilton microsyringe at a rate not exceeding of 0.2 ml/s, 2 mm deep, perpendicular to the skull surface, guided to a location approximately 0.25 mm lateral to the sagittal suture and 0.50–0.75 mm rostral to the neonatal coronary suture. Once delivery was completed, the microsyringe was left in place for 20-30 seconds before being retracted. Pups (while away from mothers) were continuously maintained in a warm environment to eliminate risk of hypothermia in

neonates. After animals received AAV injections, they were returned to the mother in their home cage. Pups were systematically kept as a group of litters. Every animal was closely monitored for signs of hypothermia following the procedure, and for days thereafter, to ensure that no detrimental side effects appear. For transduction of glutamate sensors *in vivo*, there were three- to four- weeks to suffice.

Preparation of acute hippocampal slices

Acute hippocampal slices (350 µm thick) were prepared from three- to four week-old mice. The hippocampal tissue was sliced in an ice-cold slicing solution containing (in mM): 64 NaCl, 2.5 KCl, 1.25 NaH_2PO_4, 0.5 $CaCl_2$, 7 $MgCl_2$, 25 $NaHCO_3$, 10 D-glucose and 120 sucrose saturated with 95% O_2 and 5% CO_2. Acute slices were then transferred into a bicarbonate-buffered Ringer solution containing (in mM) 126 NaCl, 3 KCl, 1.25 NaH_2PO_4, 2 $MgSO_4$, 2 $CaCl_2$, 26 $NaHCO_3$, 10 D-glucose continuously bubbled with 95% O_2 and 5% CO_2 (pH 7.4; 300–310 mOsmol). Slices were allowed to rest for at least 60 minutes before the recordings started. For recordings, slices were transferred to a recording chamber mounted on the stage of an Olympus BX51WI upright microscope (Olympus, Tokyo, Japan) and superfused at 31-33°C.

Two-photon (2P) excitation fluorescent imaging of glutamate release

2P excitation microscopy was carried out using an Olympus FV10MP imaging system optically linked to a Ti:Sapphire MaiTai femtosecond-pulse laser (SpectraPhysics-Newport) and integrated with patch-clamp electrophysiology. Acute hippocampal slices were illuminated at λ_x^{2P}=910 nm (iGluSnFr optimum) in the green emission channel. In s.radiatum of area CA1, we focused on axonal fragments which (a) were expressing the optical sensor at a level sufficient to visualise individual axonal boutons, and (b) responding to electric stimulation of Schaffer collaterals with glutamate signal. For time-lapse imaging of the iGluSnFr signal (before, during, and after evoked glutamate release), images of were collected in frame scan mode, to provide fast acquisition rates and a short pixel dwell time. Frame scans were acquired with a pixel dwell time of 0.5 µs, at a nominal resolution of ~5-7 pixels per µm (256 x 96). To minimize photodamage, only a single focal section through the region of interest containing selected axonal fragments was acquired, at a relatively low laser power (3-6 mW under the objective). The focal plane was regularly adjusted, to account for specimen drift. Time-lapse frame scans of the region of interest (containing multiple boutons in the focal plane) were acquired before and up to 60-90 min after the induction of LTP, as detailed below.

The optical signal of the iGluSnFr indicator was expressed as the $(F(t) - F_0)/F_0 = \Delta F/F_0$, where $F(t)$ stands for intensity over time, and F_0 is the baseline intensity averaged over ~150 ms prior to the stimulus.

Electrophysiology *ex vivo:* LTP induction

Glutamate release was evoked by stimulation of the bulk of Schaffer collaterals, using a concentric bipolar electrode (100 μs, 20-200 μA; corresponding to approximately one third of the saturating reponse) placed in the *s. radiatum*. Evoked field excitatory postsynaptic potentials (fEPSPs) were monitored with an extracellular recording pipette positioned in *s. radiatum* >200 μm away from the stimulating electrode. The recording electrode has a resistance of 1.5-2 MΩ when filled with a Ringer solution. fEPSPs were recorded using a Multipatch 700B amplifier controlled by the pClamp 10.2 software (Molecular Devices, USA). Synaptic responses were evoked by a brief burst of stimuli consisting of five pulses 50 ms apart (20 Hz).

Basal synaptic transmission was monitored using five-stimulus bursts applied at 0.05 Hz, for 10 to 20 min, before implementing a high-frequency stimulation (HFS) protocol for the induction of LTP. The HFS protocol included contained three trains of stimuli (100 pulses at 100 Hz) 60 s apart. GABA receptors were blocked with 100 μM picrotoxin and 3 μM CGP-52432 added to bath. The fEPSP slope was normally monitored for at least hour post-induction.

Declarations

Ethics approval

Not applicable

Consent to participate

Not applicable

Consent to publication

Not applicable

Availability of data and materials

The datasets obtained and/or analysed during the current study are available from the corresponding author on reasonable request.

Competing interests

The authors declare no competing interests.

Funding

This study was supported by the Wellcome Trust Principal Fellowship (212251_Z_18_Z), ERC Advanced Grant (323113) and European Commission NEUROTWIN grant (857562), to D.A.R.

Authors' contributions

OK carried out experimental studies, analysed the results, compiled illustrations, and contributed to manuscript writing; KZ implemented optical designed and image analyses; DAR narrated the study and wrote the manuscript

Acknowledgements

The authors thank Loren Looger and Jonathan Marvin for providing original variants of iGluSnFr.

References

1.
Hebb DO. The Organization of Behavior. New York: John Wiley & Sons; 1949.
2.
Bliss T, Collingridge G. A Synaptic Model of Memory - Long-Term Potentiation in the Hippocampus. Nature. 1993;361(6407):31–9.
3.
Bliss T, Lomo T. Long-lasting potentiation of synaptic transmission in the dentate area of the anaesthetized rabbit following stimulation of the perforant path. J Physiol. 1973;232(2):331–56.
4.
Nicoll RA. A Brief History of Long-Term Potentiation. Neuron. 2017;93(2):281–90.
5.
Huang YY, Zakharenko SS, Schoch S, Kaeser PS, Janz R, Sudhof TC. Genetic evidence for a protein-kinase-A-mediated presynaptic component in NMDA-receptor-dependent forms of long-term synaptic potentiation. Proc Natl Acad Sci U S A. 2005;102(26):9365–70. et al.
6.

Malgaroli A, Ting AE, Wendland B, Bergamaschi A, Villa A, Tsien RW. Presynaptic component of long-term potentiation visualized at individual hippocampal synapses. Science. 1995;268(5217):1624–8. et al.
7.
Emptage NJ, Reid CA, Fine A, Bliss TV. Optical quantal analysis reveals a presynaptic component of LTP at hippocampal Schaffer-associational synapses. Neuron. 2003;38(5):797–804.
8.
Kullmann DM. Amplitude Fluctuations of Dual-Component Epscs in Hippocampal Pyramidal Cells - Implications For Long-Term Potentiation. Neuron. 1994;12(5):1111–20.
9.
Isaac JT, Nicoll RA, Malenka RC. Evidence for silent synapses: implications for the expression of LTP. Neuron. 1995;15(2):427–34.
10.
Diamond JS, Bergles DE, Jahr CE. Glutamate release monitored with astrocyte transporter currents during LTP. Neuron. 1998;21(2):425–33.
11.
Luscher C, Malenka RC, Nicoll RA. Monitoring glutamate release during LTP with glial transporter currents. Neuron. 1998;21(2):435–41.
12.
Ward B, McGuinness L, Akerman CJ, Fine A, Bliss TV, Emptage NJ. State-dependent mechanisms of LTP expression revealed by optical quantal analysis. Neuron. 2006;52(4):649–61.
13.
Enoki R, Hu YL, Hamilton D, Fine A. Expression of long-term plasticity at individual synapses in hippocampus is graded, bidirectional, and mainly presynaptic: optical quantal analysis. Neuron. 2009;62(2):242–53.
14.
Lynch GS, Dunwiddie T, Gribkoff V. Heterosynaptic depression: a postsynaptic correlate of long-term potentiation. Nature. 1977;266(5604):737–9.
15.
Ibata K, Sun Q, Turrigiano GG. Rapid synaptic scaling induced by changes in postsynaptic firing. Neuron. 2008;57(6):819–26.
16.
Delvendahl I, Kita K, Muller M. Rapid and sustained homeostatic control of presynaptic exocytosis at a central synapse. Proc Natl Acad Sci U S A. 2019;116(47):23783–9.
17.
Ryan TA, Reuter H, Smith SJ. Optical detection of a quantal presynaptic membrane turnover. Nature. 1997;388(6641):478–82.
18.
Sankaranarayanan S, Ryan TA. Real-time measurements of vesicle-SNARE recycling in synapses of the central nervous system. Nat Cell Biol. 2000;2(4):197–204.
19.

Marvin JS, Borghuis BG, Tian L, Cichon J, Harnett MT, Akerboom J. An optimized fluorescent probe for visualizing glutamate neurotransmission. Nat Methods. 2013;10(2):162–70. et al.
20.
Jensen TP, Zheng K, Tyurikova O, Reynolds JP, Rusakov DA. Monitoring single-synapse glutamate release and presynaptic calcium concentration in organised brain tissue. Cell Calcium. 2017;64:102–8.
21.
Jensen TP, Zheng KY, Cole N, Marvin JS, Looger LL, Rusakov DA. Multiplex imaging relates quantal glutamate release to presynaptic Ca2 + homeostasis at multiple synapses in situ. Nature Communications 2019; 10.
22.
Reynolds JP, Zheng K, Rusakov DA. Multiplexed calcium imaging of single-synapse activity and astroglial responses in the intact brain. Neurosci Lett 2018.
23.
Jensen TP, Zheng K, Cole N, Marvin JS, Looger LL, Rusakov DA. Multiplex imaging relates quantal glutamate release to presynaptic Ca(2+) homeostasis at multiple synapses in situ. Nature communications. 2019;10(1):1414.
24.
Marvin JS, Scholl B, Wilson DE, Podgorski K, Kazemipour A, Muller JA. Stability, affinity, and chromatic variants of the glutamate sensor iGluSnFR. Nat Methods. 2018;15(11):936–9. et al.
25.
Hammond SL, Leek AN, Richman EH, Tjalkens RB. Cellular selectivity of AAV serotypes for gene delivery in neurons and astrocytes by neonatal intracerebroventricular injection. PLoS One. 2017;12(12):e0188830.
26.
Diamond JS, Jahr CE. Transporters buffer synaptically released glutamate on a submillisecond time scale. J Neurosci. 1997;17(12):4672–87.
27.
Danbolt NC, Chaudhry FA, Dehnes Y, Lehre KP, Levy LM, Ullensvang K. Properties and localization of glutamate transporters. Prog Brain Res. 1998;116:23–43. et al.
28.
Danbolt NC. Glutamate uptake. Progr Neurobiol. 2001;65:1–105.
29.
Kim JY, Ash RT, Ceballos-Diaz C, Levites Y, Golde TE, Smirnakis SM. Viral transduction of the neonatal brain delivers controllable genetic mosaicism for visualising and manipulating neuronal circuits in vivo. Eur J Neurosci. 2013;37(8):1203–20. et al.

Figures

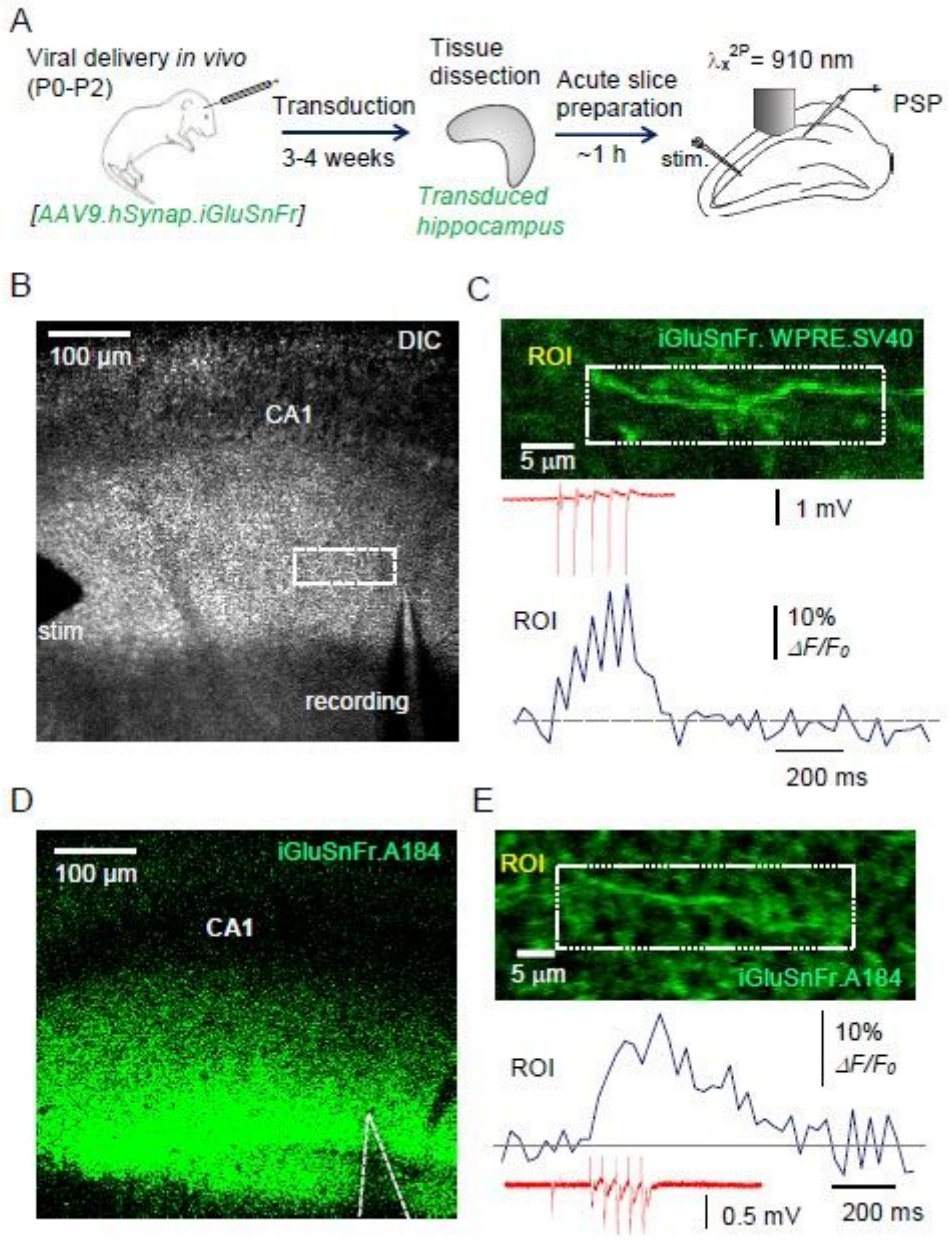

Figure 1

Monitoring glutamate release from multiple axons ex vivo in hippocampal slices labelled with iGluSnFr through viral transduction in vivo. (A) A diagram depicting viral ICV injections in neonates (P0-P2) followed by AAV transduction (3-4 weeks), dissection of hippocampi, and acute slice preparation for two-photon excitation imaging coupled with electrophysiology (Schaffer collateral stimulation and fEPSP recording in s. radiatum). (B) Experimental arrangement as seen in the microscope (DIC channel); stimulating and recording electrodes are seen; dotted rectangle, ROI for imaging. (C) Image, axon fragment in s. radiatum (ROI as in B) as seen in the green channel (AAV9.hSynap.iGluSnFr.WPRE.SV40 fluorescence; 50-frame average). Upper trace, fEPSP response to afferent stimuli (five at 20 Hz, one-trial example); lower trace, the corresponding ROI-averaged ΔF/F0 signal time course (one-trial example). (D)

Arrangement as in (B) but for the 'slow-decay' sensor variant AAV2/1.hSyn.SF.iGluSnFr.A184S (green channel shown). (E) Experiment as in (C) but for AAV2/1.hSyn.SF.iGluSnFr.A184S; notation as in (C).

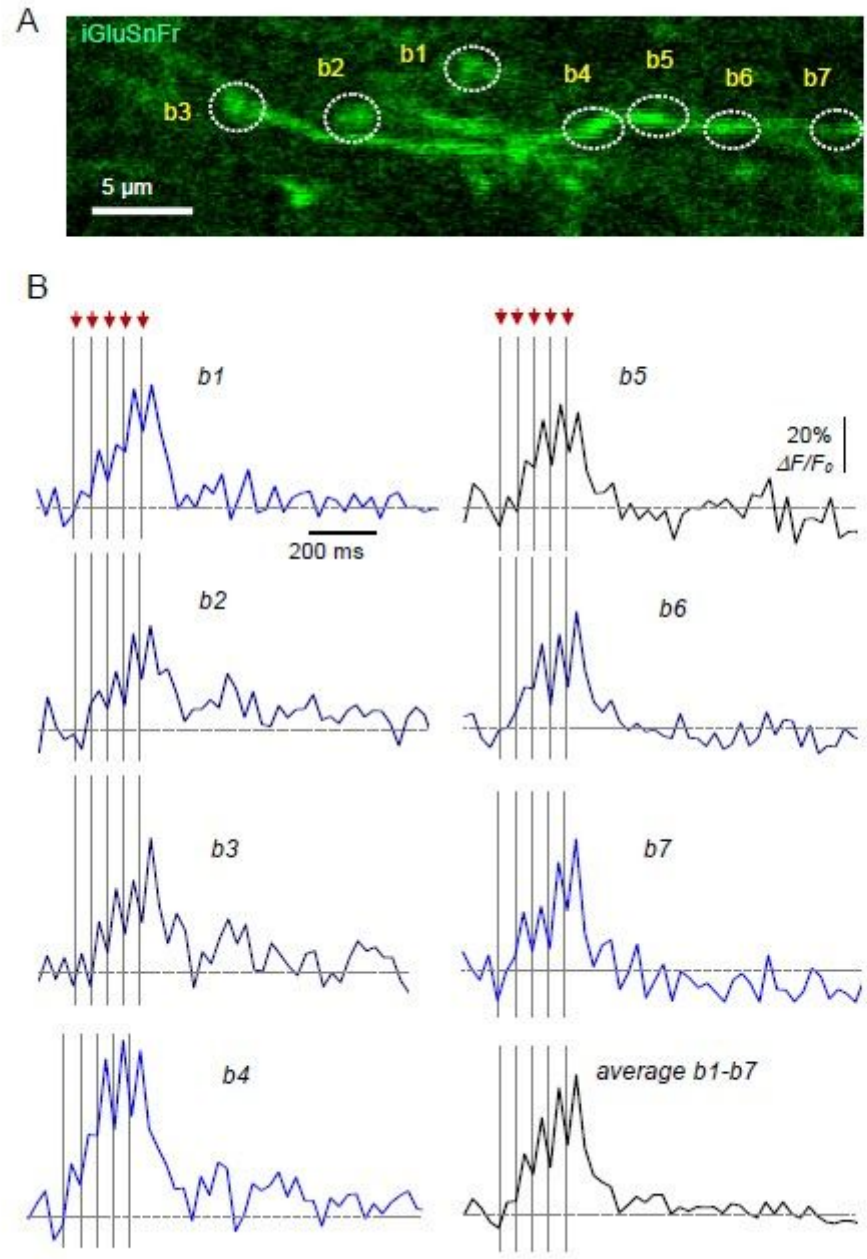

Figure 2

Optical monitoring of glutamate releases form multiple synapses using the AAV9.hSynap.iGluSnFr.WPRE.SV40 imaging in fast frame-scan mode. (A) Axonal fragments in s. radiatum (same region as in Fig. 1B), showing candidate presynaptic boutons (b1-b8), in baseline conditions (50-frame average). (B) Traces, ΔF/F0 signal time course within individual mini-ROIs that

correspond to boutons b1-b7 shown in (A), and the b1-b7 average trace, as indicated, during afferent stimulation (five pulses at 20 Hz; four-trial average).

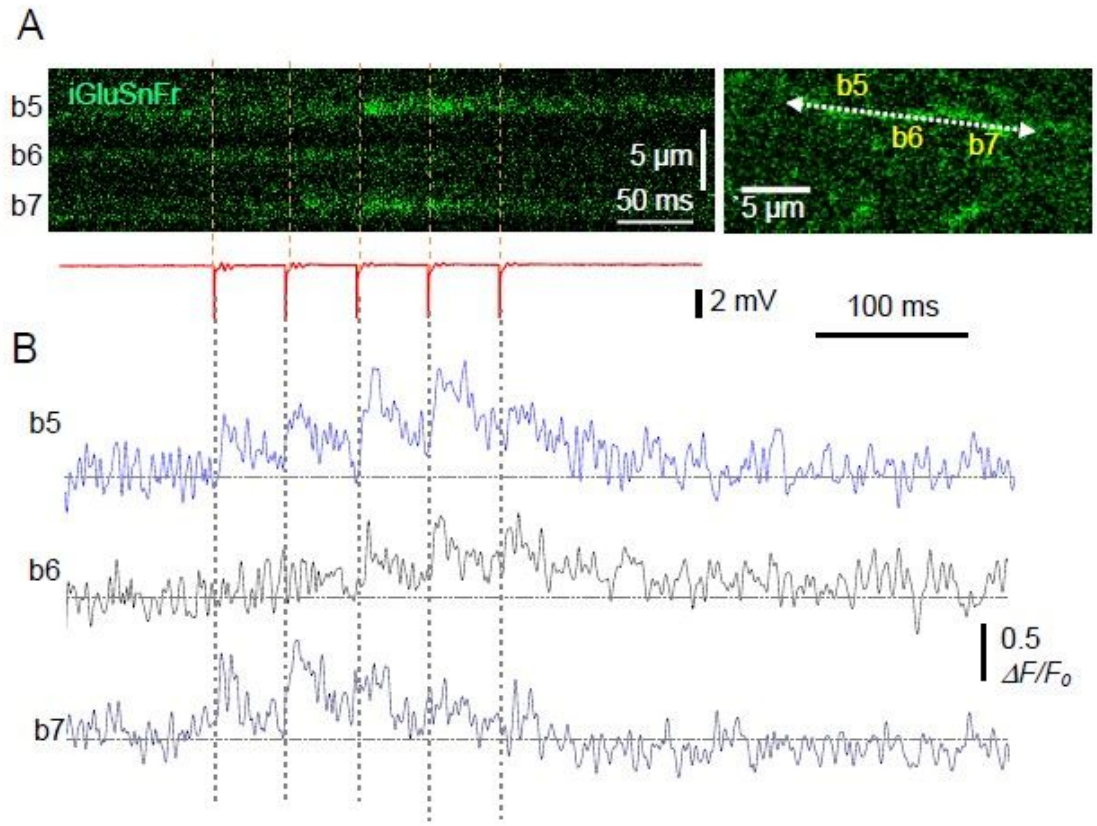

Figure 3

Documenting glutamate release from multiple axonal boutons using linescan imaging mode. (A) Linescan image (left) depicting the iGluSnFr.WPRE.SV40 fluorescence time course in three axonal boutons (b5-b7, right; ROI as in Fig. 2) during afferent stimulation (five pulses at 20 Hz), with fEPSP monitoring (red trace). (B) Traces, ΔF/F0 signal time course recorded as shown in (A) (one-trial example).

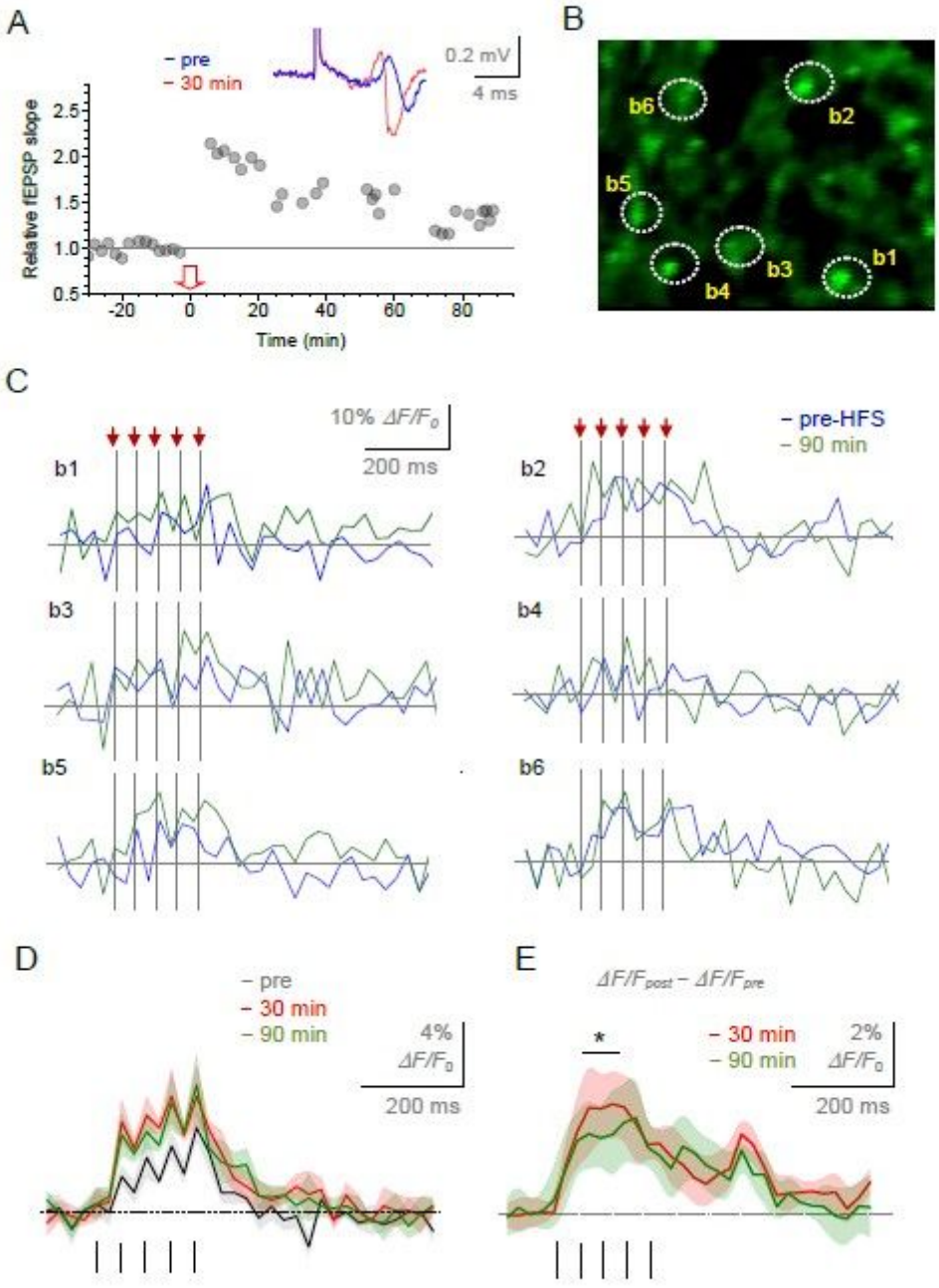

Figure 4

Glutamate release during the induction of LTP at CA3-CA1 synapses in acute slices. (A) Time course of the EPSP slope recorded in s. radiatum during LTP induction by high frequency stimulation (Methods; one-slice example). Traces, characteristic field potentials in baseline conditions (blue) and 30 min after LTP induction (red). (B) ROI in s. radiatum (iGluSnFr.WPRE.SV40 channel) showing six axonal boutons, b1-b6, designated for glutamate release monitoring. (C) iGluSnFr ΔF/F0 signal recorded from boutons b1-b6 shown in (B), before (blue; seven-trial average) and for 90 min after (green; average of 36 trials) LTP

induction; arrows and dotted lines, stimulation pulse timestamps. (D) ROI-average iGluSnFr ΔF/F0 signal (mean ± SEM band, n = 4 slices) recorded before (black), 30 min after (red), and 90 min after (green) LTP induction; vertical segments, stimulation pulse timestamps. (E) Paired-sample comparison: the difference between the ROI-average iGluSnFr ΔF/F0 signals recorded in baseline conditions, ΔF/F0 (pre), and those 30 min after (red) or 90 min after (green) LTP induction, in each of n = 4 slices; vertical segments, stimulation pulse timestamps; *p < 0.05, region with 95% confidence limits above the zero-difference line.